INTERNATIONAL JOURNAL FOR NUMERICAL METHODS IN FLUIDS, VOL. 26, 485–495 (1998)

DYNAMIC SIMULATION OF FREE SURFACES IN CAPILLARIES WITH THE FINITE ELEMENT METHOD

R. TRUTSCHEL* AND U. SCHELLENBERGER**

Department of Mechanical Engineering, Technical University of Ilmenau, D-98684 Ilmenau, Germany

SUMMARY

The mathematical formulation of the dynamics of free liquid surfaces including the effects of surface tension is governed by a non-linear system of elliptic differential equations. The major difficulty of getting unique closed solutions only in trivial cases is overcome by numerical methods. This paper considers transient simulations of liquid–gas menisci in vertical capillary tubes and gaps in the presence of gravity. Therefore the CFD code FIDAP 7.52 based on the Galerkin finite element method (FEM) is used. Calculations using the free surface model are presented for a variety of contact angles and cross-sections with experimental and theoretical verification. The liquid column oscillations are compared for numerical accuracy with a mechanical mathematical model, and the sensitivity with respect to the node density is investigated. The efficiency of the numerical treatment of geometric non-trivial problems is demonstrated by a prismatic capillary. Present restrictions limiting efficient transient simulations with irregularly shaped calculational domains are stated. © 1998 John Wiley & Sons, Ltd.

Int. J. Numer. Meth. Fluids, **26**: 485–495 (1998).

KEY WORDS: capillarity; free surface; finite elements; validation

1. INTRODUCTION

Fluid displacement in porous media, drop development and other technologies are strongly affected by surface tension resulting from molecular forces at the phase interfaces. Both the meniscus shape and the fluid motion itself are governed by these forces. Analytical approaches based on the Laplace–Young equation lead to a non-linear system of elliptic differential equations having closed solutions only in a few trivial cases which are not of practical interest. A feasible way to predict the meniscus shape and its position is numerical treatment with the finite element method (FEM) because it can easily accommodate irregular calculational domains and non-trivial boundary conditions which generally accompany three-dimensional menisci. This method was shown to be particularly effective for steady menisci in simple three-dimensional arrays of cylinders, spheres and cones forming elementary types of porous media.[1,2] The meniscus shape in polygonal capillaries in a gravity-free environment was investigated with the finite difference method (FDM).[3]

This paper presents dynamic simulations of fluid menisci in straight vertical capillary tubes and capillary gaps formed by parallel planes in a gravity environment using the Galerkin finite element method. The time-dependent meniscus motion, being initially plane and below the assumed final

* Current address: Robert Bosch G.m.b.H., Stuttgart, Germany.** Correspondence to: U. Schellenberger, Department of Mechanical Engineering, Technical University of Ilmenau, D-98684 Ilmenau, Germany.

CCC 0271–2091/98/040485–11 $17.50

Received August 1996
Revised April 1997

equilibrium position, is computed for contact angles $\vartheta = 0^\circ$ and 45° for a variety of cross-sectional dimensions. The meniscus shape is discussed and the calculational domains are extended to non-trivial cross-sections considering a prismatic capillary. The CFD code FIDAP 7.52, installed on an SGI Challenge and an SGI Indy respectively, is used.

2. THEORY

Under dynamic conditions the free surface of a fluid in a capillary intersects the capillary wall, forming a moving solid–fluid–fluid contact line. Owing to intermolecular forces, each interface is characterized by the surface tension coefficient, which gives in the equilibrium static contact angle describing the wetting condition. Figure 1 illustrates the tensions occurring at the contact line. The surface tension at curved menisci results in a local normal vector giving rise to a pressure step acting on the meniscus. This pressure step causes various physical phenomena including forced liquid motion in porous media and in thin channels. Without gravity this pressure step is constant across the meniscus, in tubes and gaps causing the surface to be spherical and cylindrical respectively. In the presence of gravity this is true only for capillaries.

The special case of vertical capillaries with constant cross-sectional area is considered here. As illustrated in Figure 2, the equilibrium position is characterized by the balance of the gravity force F_G of the rising fluid mass and the capillary force $F_C = u\sigma\cos(\vartheta)$, with the length of the intersection line u, the coefficient of surface tension $\sigma_{2,3} = \sigma$ and the contact angle ϑ. The capillary rise h is considered as the vertical distance between the base points of the menisci inside and outside the capillary which are directly connected by the same fluid.

To maintain precise experimental repeatability, a completely wetting fluid exhibiting zero contact angle is considered. To show that the computational technique works also for an incomplete wetting fluid, the case of $\vartheta = 45^\circ$ was additionally investigated. For vertical capillary tubes the governing forces are

$$F_C = \sigma 2\pi r\cos(\vartheta)$$

and, with g the gravitational acceleration and ρ the mass density,

$$F_G = \pi r^2 h\rho g + sr^2\pi\rho g - \frac{1}{3}\pi s^2\left(3\frac{r}{\cos(\vartheta)} - s\right)\rho g, \qquad s = \left(\frac{1}{\cos(\vartheta)} - \frac{1}{\cos(\vartheta)}\right)r.$$

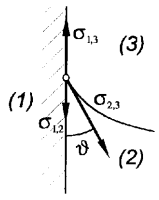

Figure 1. Wetting fluid affecting a vertical wall ($\sigma_{1,2}$, $\sigma_{1,3}$, $\sigma_{2,3}$, surface tensions; ϑ, contact angle)

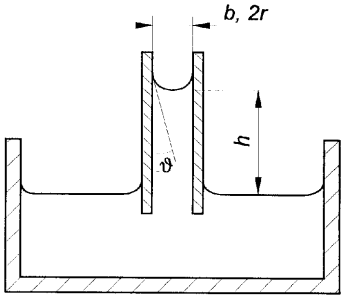

Figure 2. Capillary rise (b, gap width; r, tube radius; h, capillary rise)

The force balance at $\vartheta = 0^\circ$ gives for the capillary rise

$$h = \frac{2\sigma - r^2\rho g + \frac{2}{3}r^2\rho g}{r\rho g}, \tag{1}$$

whereas for $\vartheta = 45^\circ$ the capillary rise becomes

$$h = \frac{\sqrt{2}\sigma - (\sqrt{2}-1)r^2\rho g + \frac{1}{3}(\sqrt{2}-1)^2 r^2(2\sqrt{2}+1)\rho g}{r\rho g}. \tag{2}$$

For the capillary rise in a gap formed by two parallel vertical walls of length a, these forces are

$$F_C = \sigma 2a\cos(\vartheta)$$

and

$$F_G = bha\rho g + \frac{b^2}{2}a\rho g - \frac{b^2}{8\cos^2(\vartheta)}\left[\pi\left(1 - \frac{\vartheta}{90^\circ}\right) - \sin(2\vartheta)\right]a\rho g.$$

Hence, for $\vartheta = 0^\circ$,

$$h = \frac{2\sigma - (b^2/2)\rho g + \frac{1}{8}\pi b^2\rho g}{b\rho g}. \tag{3}$$

The rising meniscus reaches the final position after a free, damped oscillation. Assuming small displacements of the liquid column, its dynamic behaviour is comparable with that of a linear mechanical spring–damper–mass system, being a harmonic oscillator. The natural frequencies of the damped and undamped systems, f and f_0 respectively, are, with the damping coefficient D,

$$f_0 = \frac{1}{2\pi}\sqrt{\left(\frac{g}{h}\right)}, \qquad f = f_0\sqrt{(1-D^2)}. \tag{4a, b}$$

This approach has usually proved adequate when the length of the fluid in the capillary is large compared with the tube diameter; however, deviations from the expected behaviour have been observed even when this condition is satisfied.[4] The fluid in a capillary is at one end bound by a free meniscus where the velocity field and the viscous and interial forces differ strongly from the assumed Poiseuille flow. This may affect the dynamics significantly. As reported in the following sections, the damping coefficient assuming Poiseuille flow is much lower than the computed motion shows.[5] To improve the mechanical model, the computed damping coefficient may be used instead of Poiseuille flow one. This coefficient is obtained from the ratio of two consecutive amplitudes s_{n-1} and s_n:

$$D = \frac{\xi}{\sqrt{(\xi^2 + \pi^2)}}, \qquad \xi = \ln\left|\frac{s_{n-1}}{s_n}\right|. \tag{5}$$

3. EXPERIMENTAL

The experimental investigation of the capillary rise was performed for four capillary tubes with $d = 1{\cdot}50$, $1{\cdot}67$, $1{\cdot}88$ and $2{\cdot}42$ mm and four capillary gaps with $b = 1{\cdot}1$, $1{\cdot}4$, $1{\cdot}5$ and $2{\cdot}0$ mm in distilled water. The capillary rise was measured optically as shown in Figure 3. A beaker containing distilled water is movable by a vertical linear bearing. Exact positioning with simultaneous determination of the distance moved was performed by a micrometer. The wetting fluid rises in the capillary when the latter is positioned and fixed in the beaker as shown. The fluid column takes only a few seconds to reach the steady state position after an initial damped oscillation. To get the fluid completely wetting, the glass pieces were degreased with acetone, refined with chromic sulphuric

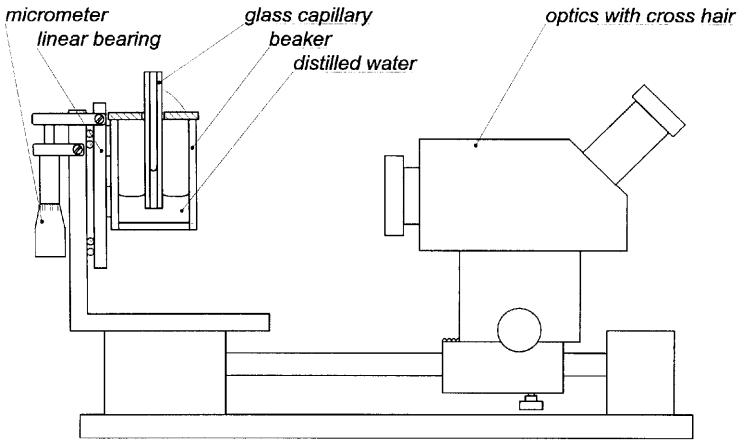

Figure 3. Configurations for measuring capillary rise in tubes

acid and finally rinsed several times with distilled water. Using the micrometer, the base points of both menisci and the cross-hair were zeroed. The distance moved represented the capillary rise.

The tube and gap dimensions were determined using a microscope. The relative deviation between the inner tube diameters at both surface ground sides was found to be $\Delta b/b \leqslant 2\%$. The deviation of the gap width was $\Delta b/b \leqslant 3\%$. Only the inner range of approximately 20 mm of the 40 mm long gap walls could be used for the determination of the capillary rise, because this regions remains nearly unaffected by the open gap ends where a meniscus fall occurs. The relative measurement error was determined to be $\Delta h/h = 3{\cdot}5\%$, mainly caused by the irregular capillary shapes mentioned above, by the meniscus curvature in the beaker (pressure step) and by deviations in the optical focusing.

4. CALCULATIONS

4.1. Finite element approach

Simulations of moving fluids bound partly by a free surface, including the effects of surface tension, may be carried out in FIDAP 7.52 using the *free surface model*. Such phase change configurations of immiscible fluids are mathematically described by the Navier–Stokes equations with additions to include the kinematics and the interfacial tension. These equations were solved with the *segregated solver* and the *backward Euler time integration scheme*.

The simulation was carried out transiently, requiring higher computational cost but improving the convergence characteristics significantly. The fluid was assumed to be a Newtonian one and incompressible, with the free surface being initially specified to be plane and positioned below the assumed final position. The computational domain involved only the rising fluid, neglecting the gaseous phase. At the contact line the slip condition was imposed. In the case of zero contact angle a severe convergence problem occurs, because this boundary condition and the node location of the corner elements are mutually exclusive. This problem was overcome by the use of quadratic elements, making the mathematical formulation more flexible but leading to a more complex mathematical model. The following parameters were used for the simulations: $\rho = 998{\cdot}4$ kg m^{-3}, $g = 9{\cdot}81$ m s^{-2}, $\sigma = 0{\cdot}0725$ N m^{-1}, $\eta = 0{\cdot}001$ Pa s (η is the dynamic viscosity).

4.2 Dynamic simulation of capillary rise in tubes

To gain experience for future, for more complex problems, the simulations of capillary tubes were carried out three-dimensionally. As illustrated in Figures 4 and 6, the z-displacement of the inner surface node is taken as the capillary rise. Because of the element topology in the case of $\vartheta = 45°$, this node is not placed exactly on the apex; however, assuming a spherical meniscus, the deviation in the z-direction remains less than 1% and need not be taken into account.

Tending towards the equilibrium state, initially the fluid near the surface moves, oscillating to shape the meniscus, as Figures 5 and 7 reveal. Subsequently the complete liquid column oscillates damped to the final equilibrium position characterized by a much lower frequency because of the larger fluid mass involved but driven by the same capillary force. It is observed that the damping coefficient increases with decreasing diameter and decreasing contact angle.

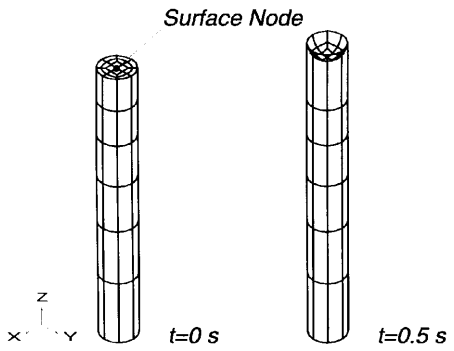

Figure 4. FE model, $d = 1{\cdot}88$ mm, $\vartheta = 0°$

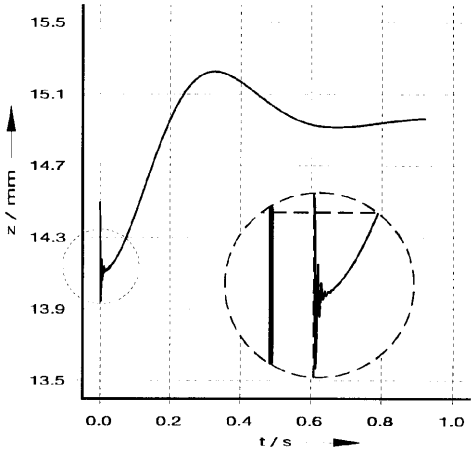

Figure 5. Computed $z(t)$-displacement

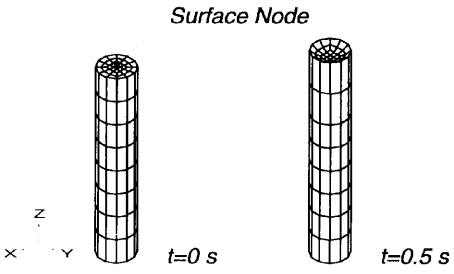

Figure 6. FE model, $d = 1{\cdot}88$ mm, $\vartheta = 45°$

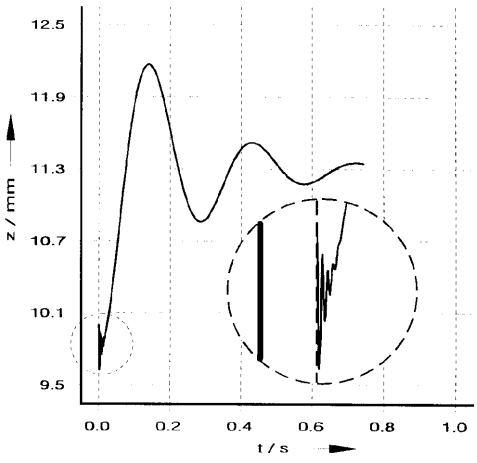

Figure 7. Computed $z(t)$-displacement

Convergence instability occurs when attempting to increase the time steps substantially after attenuation of the meniscus oscillation. This numerical phenomenon caused up to 20,000 small time steps and an unexpectedly high computational time for the complete simulation, especially in the case of $\vartheta = 0°$. Consequently, only two capillary tubes were simulated for that case. The case of $\vartheta = 45°$ was additionally simulated because of a smaller number of elements and element distortions, resulting in faster simulations. For the tube with $d = 2{\cdot}42$ mm the CPU requirements were $t_{\text{sim}} = 16{\cdot}6$ CPU hours (case $\vartheta = 45°$) and $t_{\text{sim}} = 179{\cdot}5$ CPU hours (case $\vartheta = 0°$). Although this is a simple problem in terms of the geometry and physics, the approach is general and may be extended to more complex simulations.

Serious convergence problems occurred when trying to reduce the domain of a semi-cross-section discretized with axisymmetric elements owing to their highly non-linear mathematical formulation.

4.3. Dynamic simulation of capillary rise between parallel vertical walls

A two-dimensional finite element model was used to simulate the capillary rise in gaps between parallel vertical walls. This reduced model required much less simulation time, in the range of $t_{\text{sim}} = 4$–8 CPU hours.

Figure 8 shows the surface node motion. The meniscus performs qualitatively the same dynamics as for tubes. Differences from the simulations above exist in that the initial meniscus oscillation is more damped than in tubes.

4.4. Discussion of results

The values for the capillary rise in tubes are summarized in Figure 9. For a wetting fluid with $\vartheta = 0°$ the values obtained by the FEM are 3% lower than those obtained by equation (1). The deviation between the numerical and measured values is 3%, being well within the range of maximum measurement deviation. In the case of an incomplete wetting fluid characterized by $\vartheta = 45°$, the values obtained by the FEM are 2% higher than those obtained by equation (2).

The values for the capillary rise in gaps are summarized in Figure 10. The values obtained by the FEM and by equation (3) differ by less than 1·8%, with lower numerical values than the tube simulation. The values obtained by the FEM and by experimental investigations differ by 3·5%, also

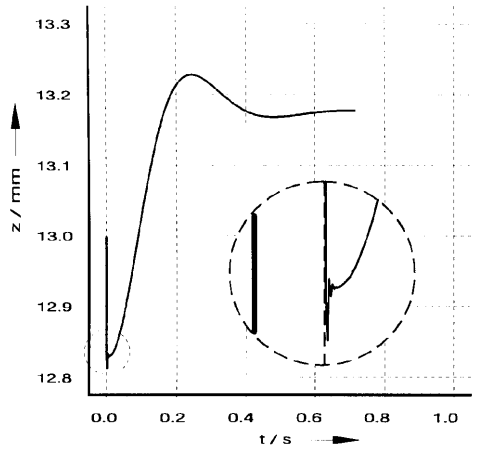

Figure 8. Computed $z(t)$-displacement for $b = 1{\cdot}10$ mm

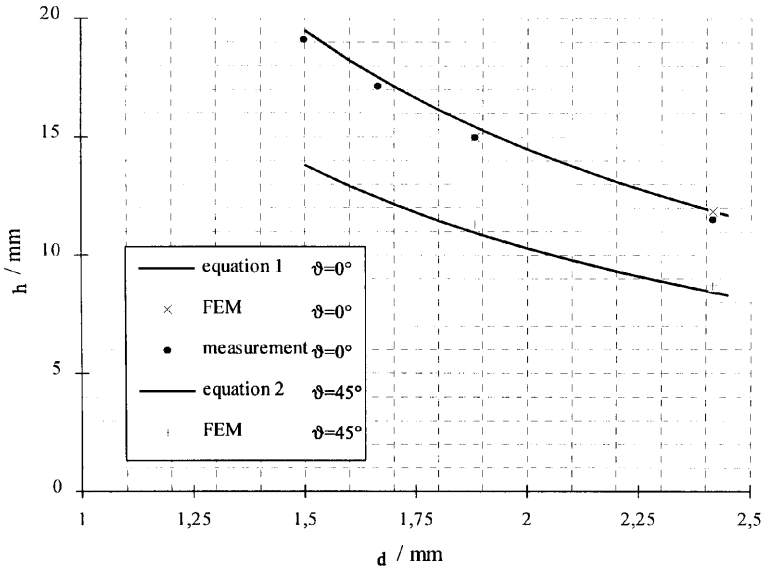

Figure 9. Capillary rise in tubes, $\vartheta = 0°$ (upper curve) and $\vartheta = 45°$ (lower curve)

being within the range of maximum measurement deviation. In both cases the simulation results are in good agreement with the measurements and theory.

The dynamic behaviour is discussed on the basis of the natural frequencies summarized in Table I. It is found that the theoretical natural frequencies of the undamped system given by equation (4a) are up to 26% higher than the computed values. Using the computed damping coefficient in equation (4b), the natural frequencies decrease but significant differences of up to 25% remain.

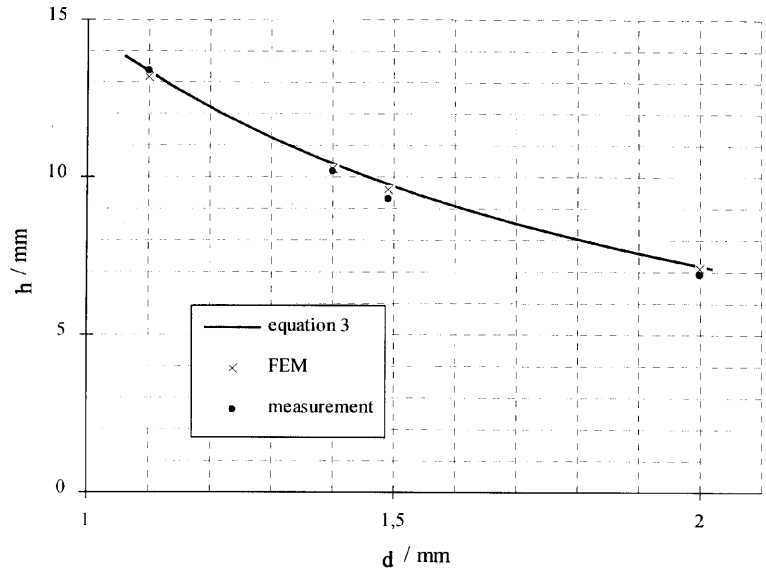

Figure 10. Capillary rise in gaps, $\vartheta = 0°$

Table I. Natural frequencies of column oscillation

	$\vartheta = 45°$		$\vartheta = 0°$	
	$d = 1{\cdot}88$ mm	$d = 2{\cdot}42$ mm	$d = 1{\cdot}88$ mm	$d = 2{\cdot}42$ mm
Equations 4(a, b), 5	4·58 Hz	5·27 Hz	3·72 Hz	3·97 Hz
FEM	3·48 Hz	3·98 Hz	2·97 Hz	3·41 Hz
Deviation	24·0%	24·5%	20·2%	12·23%

This manifests the model defects reported by Tilton.[4] On the other hand, the very high number of time steps required for reasonable convergence may lead to a numerical problem. More investigations are necessary to clarify this result, including experimental work. Considering the defects of the model for comparison, this result is taken as confirmation of the simulation.

4.5. Mesh refinement

The simulation was repeated for one capillary gap using a refined mesh to investigate the solution stability. Figure 11 depicts both meshes and the results.

This modification decreased the capillary rise and the natural frequency of column oscillation by about 1·5% and 3% respectively. These deviations are comparably small, so the realized coarse element mesh is considered to be stable for a wide range of practical problems and may be used for fast initial simulations.

4.6. Meniscus curvature

The steady state shape of free surfaces tends to an energy minimum with respect to the gravitational potential and the surface energy. This section considers the meniscus curvature of a completely wetting fluid in capillary gaps. In the absence of gravity the magnitude of the curvature radius has to be constant, causing a semicylindrical meniscus.

In Figure 12 a circular approach formed by the intersection nodes and the base point nodes, by all computed node positions themselves and the theoretical semicylindrical meniscus are depicted. The

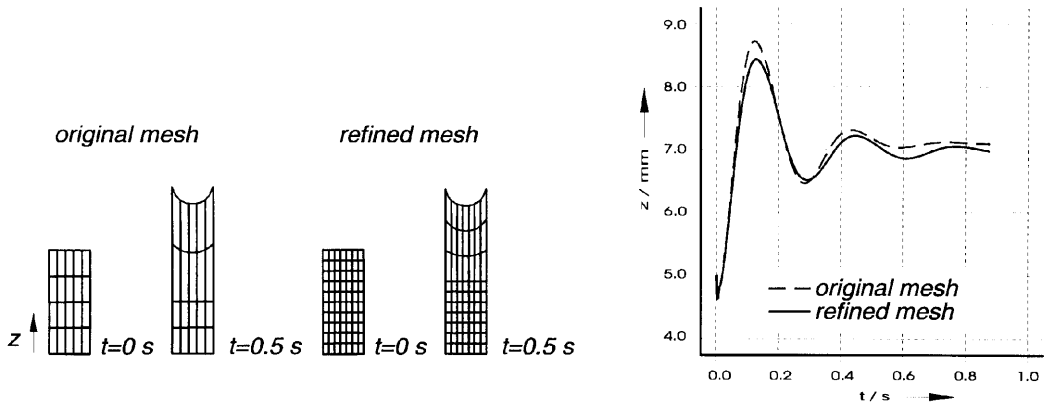

Figure 11. Node density dependence for solution variables of case $b = 2$ mm

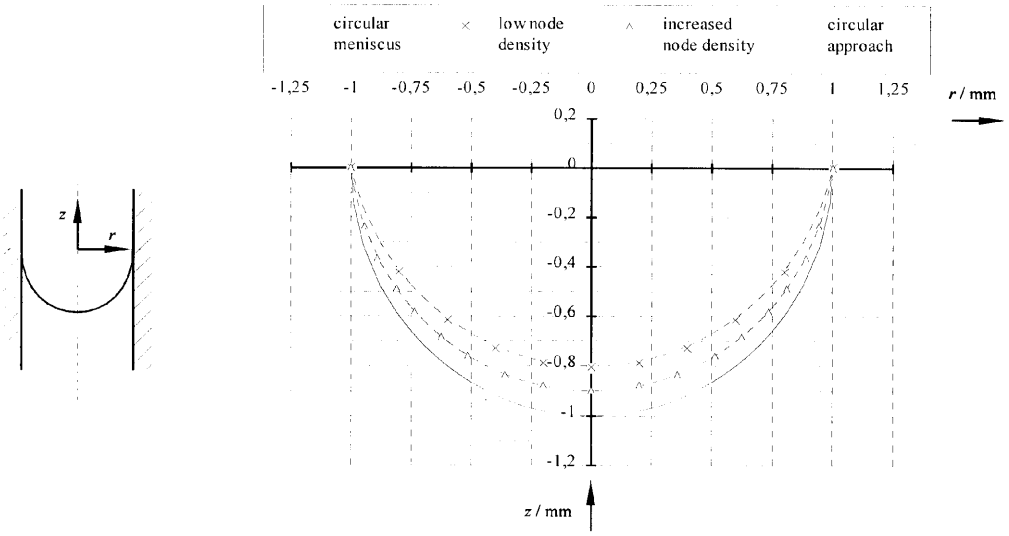

Figure 12. Meniscus curvature in a capillary gap with $b = 2$ mm

corner positions are zeroed. Obviously, use of the FEM leads to a circular meniscus with larger radius than theoretically assumed. If the node density is increased in both dimensions, the meniscus tends to be more semicylindrical. Note that small elements near the intersection line cause large defects and destabilize the solution, limiting the node density to resolve physical details near the contact line. An additional simulation with $b = 1{\cdot}1$ mm resulted in a qualitatively identical curvature. To investigate the influence of gravity, a capillary closed at the bottom was modelled in a gravity-free environment. The resulting meniscus shape varied only slightly, indicating that the meniscus shape in capillaries is independent of gravitational forces.

4.7. Dynamic simulation of capillary rise in a capillary of rectangular cross-section

Besides the special cases discussed above, in the focus of scientific and practical interest are fluid motions in channels of variously shaped cross-sections. In this section the dynamic rise in a rectangular capillary with an aspect ratio of two is considered (Figure 13). To minimize the computation time, the contact angle was set to $\vartheta = 45°$.

Significant initial and main oscillations are also observed for this case (Figure 14). In contrast with the simulations above, the initial oscillation is composed of more than one harmonic oscillation. As

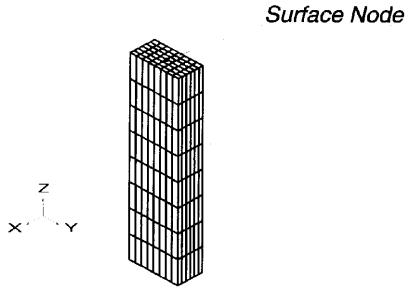

Figure 13. FE model of a prismatic capillary

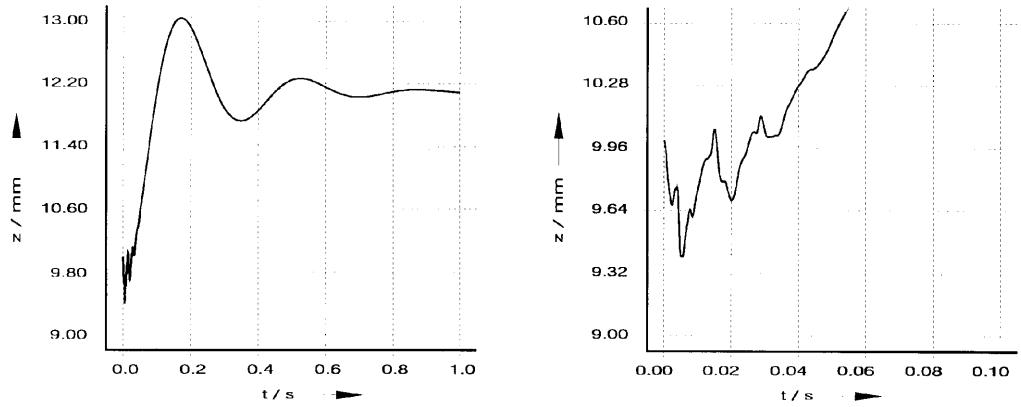

Figure 14. Computed $z(t)$-displacement of the surface node

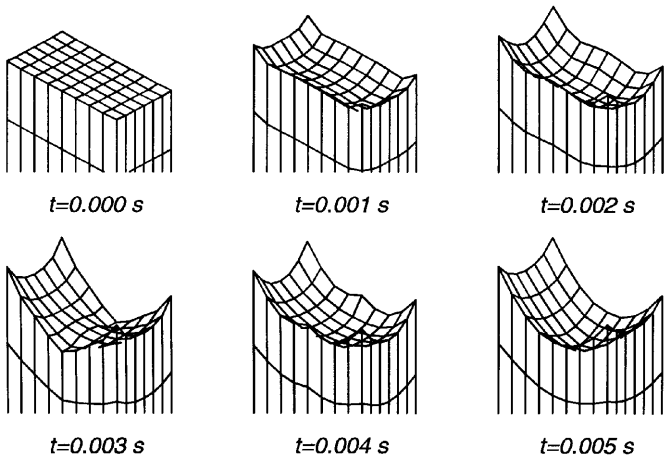

Figure 15. Meniscus shape at various stages of initial phase

shown in Figure 15, the contact angles reach their steady values first, resulting in a force imbalance and initiating the initial meniscus oscillation.

5. CONCLUSIONS

The power of the finite element method for predicting and analysing transient meniscus configurations without substantial geometrical and physical simplifications has been demonstrated. Good agreement with theoretical predictions and experiments (with a maximum deviation of 3%) was found in the numerical determination of the capillary rise in tubes and gaps. Stable solutions require decreased convergence limits if large element distortions occur. This restricts refinements of the structured mesh to resolve details near the contact line. However, mesh refinement affects the dynamics and the capillary rise only slightly, allowing coarse meshes to be a good basis for qualitative and quick simulations.

The initially plane meniscus oscillates much faster to reach the equilibrium position than the liquid column does, as qualitatively confirmed by experiments. The frequency of the oscillating fluid column differed from the mechanical model, which may be caused by defects of the mechanical model. One focus of further experiments should be the verification of the column frequency. It could be manifested that the shape of the meniscus in capillary gaps is cylindrical and independent of gravitational forces. Generally the numerical accuracy may be improved by increasing the node density but it is limited by increasing element deformations in the corner region resulting in convergence problems.

The presented transient simulations on basic capillaries based on a commercial CFD code may be extended to capillaries with more complex cross-sections when large distortions do not occur. Nevertheless, considering the potential of this approach, it seems to be a good basis for handling a wide range of scientific and engineering problems in future simulations.

REFERENCES

1. F. M. Orr Jr., L. E. Scriven and A. P. Rivas, 'Menisci in arrays of cylinders: numerical simulation by finite elements', *J. Colloid Interface Sci.*, **52**, 602–610 (1975).
2. F. M. Orr Jr., R. A. Brown and L. E. Scriven, 'Three-dimensional menisci: numerical simulation by finite elements', *J. Colloid Interface Sci.*, **60**, 137–147 (1976).
3. H. Wong, S. Morris and C. J. Radke, 'Three-dimensional menisci in polygonal capillaries', *J. Colloid Interface Sci.*, **148**, 317– 336 (1991).
4. J. N. Tilton, 'The steady motion of an interface between two viscous liquids in a capillary tube', *Chem. Engng. Sci.*, **43**, 1371– 1382 (1988).
5. R. Trutschel, 'Berechnung der instationären Bewegung von freien Oberflächen zur Modellbildung eines Flüssigkolben-Stirlingmotors', *Diplomarbeit*, Fakultät für Maschinenbau, TU Ilmenau, 1996.
6. G. Mason and N. R. Morrow, 'Meniscus curvature in capillaries of uniform cross-section', *J. Chem. Soc.*, **00**, 2375–2393 (1983).
7. S. Ramakrishnan and S. Hartland, 'Effect of contact angle on capillary rise in annular meniscus', *J. Colloid Interface Sci.*, **80**, 497–507 (1980).

